Article:

Söderström, P. A., Jaworski, G., Valiente Dobón, J. J. et al. (22 more authors) (2019) Neutron detection and γ-ray suppression using artificial neural networks with the liquid scintillators BC-501A and BC-537. Nuclear Instruments and Methods in Physics Research, Section A: Accelerators, Spectrometers, Detectors and Associated Equipment. pp. 238-245. ISSN 0168-9002

https://doi.org/10.1016/j.nima.2018.11.122

Neutron detection and γ-ray suppression using artificial neural networks with the liquid scintillators BC-501A and BC-537

P.-A. Söderström[a,b,c,d,*], G. Jaworski[e,f,g], J. J. Valiente Dobón[e], J. Nyberg[d], J. Agramunt[h], G. de Angelis[e], S. Carturan[e], J. Egea[i,h], M.N. Erduran[j], S. Ertürk[k], G. de France[l], A. Gadea[h], A. Goasduff[e], V. González[i], K. Hadyńska-Klęk[e], T. Hüyük[h], V. Modamio[e], M. Moszynski[m], A. Di Nitto[n,o], M. Palacz[g], N. Pietralla[b], E. Sanchis[i], D. Testov[p], A. Triossi[e], R. Wadsworth[q]

[a] *Extreme Light Infrastructure-Nuclear Physics (ELI-NP), 077125 Bucharest-Măgurele, Romania*
[b] *Institut für Kernphysik, TU Darmstadt, D-64289 Darmstadt, Germany*
[c] *GSI Helmholtzzentrum für Schwerionenforschung GmbH, 64291 Darmstadt, Germany*
[d] *Department of Physics and Astronomy, Uppsala University, SE-75120 Uppsala, Sweden*
[e] *Laboratori Nazionali di Legnaro dell'INFN, I-35020 Legnaro (Padova), Italy*
[f] *Faculty of Physics, Warsaw University of Technology, ul. Koszykowa 75, 00-662 Warszawa, Poland*
[g] *Heavy Ion Laboratory, University of Warsaw, ul. Pasteura 5A, 02-093 Warszawa, Poland*
[h] *Instituto de Física Corpuscular, CSIC-Universidad de Valencia, E-46071 Valencia, Spain*
[i] *Department of Electronic Engineering, Universidad de Valencia, E-46071 Valencia, Spain*
[j] *Faculty of Engineering and Natural Sciences, Istanbul Sabahattin Zaim University Istanbul, Turkey*
[k] *Niğde Ömer Halisdemir University, Fen-Edebiyat Falkültesi, Fizik Bölümü, Niğde, Turkey*
[l] *GANIL, CEA/DSAM and CNRS/IN2P3, Bd Henri Becquerel, BP 55027, F-14076 Caen Cedex 05, France*
[m] *National Centre for Nuclear Research, A. Soltana 7, PL 05-400 Otwock-Swierk, Poland*
[n] *INFN Sezione di Napoli, I-80126 Napoli, Italy*
[o] *Johannes Gutenberg-Universität Mainz, 55099 Mainz, Germany*
[p] *Dipartimento di Fisica e Astronomia and INFN, Sezione di Padova, Padova, Italy*
[q] *Department of Physics, University of York, Heslington, York, YO10 5DD, UK*

[*] Corresponding author
Email address: `par.anders@eli-np.ro` (P.-A. Söderström)

Preprint submitted to Nuclear Instrument and Methods in Physics Research A *November 24, 2018*

Abstract

In this work we present a comparison between the two liquid scintillators BC-501A and BC-537 in terms of their performance regarding the pulse-shape discrimination between neutrons and γ rays. Special emphasis is put on the application of artificial neural networks. The results show a systematically higher γ-ray rejection ratio for BC-501A compared to BC-537 using the traditional charge comparison method. Using the artificial neural network approach the discrimination quality was improved to more than 95% rejection efficiency of γ rays over the energy range 150 to 1000 keV for both BC-501A and BC-537. However, due to the larger light output of BC-501A compared to BC-537, neutrons could be identified in BC-501A using artificial neural networks down to a recoil proton energy of 800 keV. The corresponding low-energy limit for BC-537 was at a recoil deuteron energy of 1200 keV. We conclude that it is possible to obtain the same γ-ray rejection quality from both BC-501A and BC-537 for neutrons above a low-energy threshold. However, this threshold is lower for BC-501A which is important for nuclear structure spectroscopy experiments of rare reaction channels where low-energy interactions dominates.

Keywords: BC-501A, BC-537, digital pulse-shape discrimination, fast-neutron detection, liquid scintillator, neural networks
PACS: 29.40.Mc, 29.85.Ca

1. Introduction

One of the on-going advances in the field of nuclear physics is the construction and operation of several large facilities. These facilities will focus on providing users with high quality radioactive- and high-intensity stable ion-beams, γ-ray beams or particle beams for nuclear physics experiments. Within the nuclear structure framework of these facilities, γ-ray spectroscopy of atomic nuclei will be performed using advanced γ-ray spectrometers to study nuclei of interest with high precision. These spectrometers will be complemented with ancillary detectors for reconstructing and identifying weak reaction channels [1–6]. For the studies of very neutron deficient nuclei, one experimental strategy is through heavy-ion induced fusion-evaporation reactions with low proton and α particle multiplicities, one or less, and emission of, usually, up to three neutrons [7–12]. A typical example of the kind of setup used to identify these reaction products is shown in Fig. 1.

[Figure 1 about here.]

For the feasibility of this kind of experiment to reach even further out into the exotic nuclei than before, new and advanced γ-ray spectrometers [15], charged particle detectors [16], and neutron multiplicity-filters are being constructed. These new detectors take advantage of the possibilities accompanying the advent of the digital electronics era to get pure reaction-channel selection with high-efficiency. Two examples of next generation neutron detectors, with different approaches, are DESCANT (DEuterated SCintillator Array for Neutron Tagging) [17] at TRIUMF, based on deuterated liquid scintillator detectors, and NEDA (NEutron Detector Array) [13, 18], made from regular hydrogen-based liquid scintillator detectors.

For the technical design of the European detector system, NEDA, several parameters have been optimized, such as the size and shape of individual detectors [19], choice of detector material, photomultiplier tubes [20, 21] the geometry of the detector array [13], electronics [22–24] and algorithms for pulse-shape discrimination [25, 26]. These parameters are not independent from each other but correlated in various aspects. For example, the geometry of the detector needs to be designed to minimize the probability that one neutron will scatter and induce signals in more than one detector, $P_{1\text{n}\to2\text{n}}$. In addition, the quality of this $P_{1\text{n}\to2\text{n}}$ rejection is known to have a strong dependency on the quality of discrimination between neutrons and γ rays [27, 28]. Furthermore, the efficiency of the detector for detecting low-energy neutrons will depend on the quantum efficiency of the photomultiplier tube, which will also influence the discrimination between neutrons and γ rays. Thus, the optimal performance of one parameter, for example neutron-γ discrimination, is not only important for that particular aspect of the detector system but the detection power of the system as a whole.

The aim of the work presented in this paper is the investigation of two aspects of neutron-γ discrimination: a comparison of the pulse-shape properties of regular and deuterated liquid scintillators BC-501A and BC-537, and how the application of Artificial Neural Networks (ANNs) can be used to improve the discrimination properties. For this particular study, these two liquid scintillators were chosen since the BC-501A scintillator is being used in the NEDA detector array [13] and BC-537 is the scintillator of choice for DESCANT [17].

2. Scintillators

The two liquid scintillators compared in this paper are BC-501A, which is the standard type of liquid scintillator often used in this type of instruments, and BC-537 that has gained attention in recent years as a possible alternative. For detailed comparisons between these scintillators and their properties, see for example Refs. [19, 29, 30]. Xylene-based BC-501A, $C_6H_4(CH_3)_2$, has a light output that is about 78% of anthracene and a hydrogen to carbon ratio of 1.287. It has three decay components with 3.16 ns, 32.3 ns and 270 ns decay times [31]. BC-537 is made of purified deuterated benzene, C_6D_6, and has a light output that is about 61% of anthracene. BC-537 has a deuterium to carbon ratio of 0.99 and a deuterium to hydrogen ratio of 114. The decay components of BC-537 are not listed in the data sheet, but also consist of a fast and slow part with similar time scales, as shown in Fig. 2. The details of this figure are discussed in section 5.

[Figure 2 about here.]

The scintillation light is produced by the energy transfer of the incoming particles with the scintillator material in the detector. In the case of neutrons and γ rays, the γ rays only interact with the electrons in the liquid, while the energy loss of the neutrons is based on nuclear collisions either with the protons or deuterons, and to a minor degree with the carbon nuclei. For both scintillators, the relative amount of light produced from the faster and slower decay components depend on the radiation species. In particular, the light from the fast component is quenched for interacting particles with large stopping power (protons or deuterons) relative to particles with small stopping power (electrons). This property is the basis for the pulse-shape discrimination between neutrons and γ rays.

It is known since long that the angular distribution in proton-neutron scattering is isotropic while the deuteron-neutron scattering cross-section is peaked in backwards and forwards directions [32]. It has been suggested that the scattering kinematics of BC-537 may create an additional correlation between the neutron energy and light production which can be used as further information for $P_{1n\to 2n}$ rejection. This property could make it an option to use, instead of BC-501A, in neutron detector arrays, despite the lower light output [17, 29]. However, it was shown [33] that whilst the significantly increased cross-section for forward and backward scattered neutrons on deuterons plays a role in small detectors the effect is blurred out for large volume, NEDA-like detectors, see Ref. [19].

3. Experiment

In this work, four detectors, two filled with BC-501A and two filled with BC-537, all of cylindrical shape with a size of $5'' \times 5''$ were used. The detectors were coupled to 10-stage photomultiplier tubes of the type Philips XP4512B with a $5''$ diameter with voltage dividers of the type Photonics VD105K (see Ref. [34] for a comparative study of this kind of photomultiplier tube in relation to other common photomultiplier tubes). Each detector was surrounded by a teflon expansion tube to avoid the formation of overpressure air bubbles inside the container, within a 1 mm external housing. A $3'' \times 3''$ BaF_2 detector was also used as time reference for time-of-flight (TOF) measurements. Data sets were collected by triggering on a coincidence between at least one of the two neutron detectors and the BaF_2 detector.

The signals from the detectors were split into a digital and an analogue data acquisition system using a linear Fan-In/Fan-Out (FIFO) unit. The analogue pulse-shape discrimination was carried out using a BARTEK NDE202 unit[1], of the same type as is used in the Neutron Wall detector array [35]. For the TOF measurement a TAC was used with the constant fraction discriminator (CFD) of the BaF_2 signal as start and the CFD of one of the neutron detector signals as stop. The digitizers communicated with the data acquisition system via a VME computer bus standard controller using an optical link. The original data acquisition control software [38] was modified for this purpose.

To digitize the signals from the detectors and accompanying analogue electronics, two digitizers from Struck Innovative Systems were used. One digitizer was a SIS3350 unit [36] which has four channels with a sampling frequency of 500 MS/s and a bit resolution of 12 bits. This sampling frequency and bit resolution has been shown to be sufficient for pulse-shape analysis of the signals from liquid scintillator detectors [25]. The other digitizer, used for the signals from the time-to-amplitude converters (TACs) and the analogue pulse-shape discrimination unit, was SIS3302 [37]. This unit has eight channels with a sampling frequency of 100 MS/s and a resolution of 16 bits.

[1] The NDE202 was built by D. Wolski, M. Moszyński, et al. at The Andrzej Soltan Institute for Nuclear Studies, Swierk, Poland

The reason for using the SIS3302 unit was to synchronize the analogue and digital data acquisition systems.

The data were collected using several γ-ray sources, listed in Table 1, and a ^{252}Cf neutron source with an activity of approximately 1.3 MBq at the time of the experiment. The data from each source was collected separately. For the pulse-shape analysis the spontaneous fission of the ^{252}Cf provided both the neutrons and γ rays for the data set. An overview of the experimental set-up is illustrated in Fig. 3.

[Figure 3 about here.]

[Table 1 about here.]

4. Calibration

One of the main aims of the NEDA project is to obtain an instrument with a high efficiency for detection of low-energy neutrons. Due to this, the techniques to discriminate between neutrons and γ rays, further discussed in section 5, have to be especially evaluated at low energy. It is also primarily in the low-energy region where the signal shapes of neutrons and γ rays become more difficult to be distinguished from each other because of low statistics of photoelectrons involved in the process.

Due to the low Z of the liquid scintillators, an energy calibration using the full-energy deposition peak from known sources is in most cases not feasible except for sources with very low γ-ray energy. Instead, the positions of the Compton edges, E_{ce}, in the γ-ray spectra collected with the were used

$$E_{\mathrm{ce}} = E\left(1 - \frac{1}{1 + \frac{2E}{m_{\mathrm{e}}c}}\right), \tag{1}$$

with E being the γ-ray energy and m_{e} being the electron mass. The speed of light, c, was taken equal to 1. The locations of the Compton edges for the sources used in this work are listed in Table 1. However, the correspondence between the features observed in the uncalibrated spectrum, the Compton distribution, and the actual Compton edge according to Eq. (1), is less straightforward compared to using the full-energy deposition peak for calibrations.

A detailed study of the Compton edge position with respect to the Compton distribution was carried out in Ref. [39] on the scintillator NE-213 with a composition similar to the BC-501A. In that reference the response curve of electrons of fixed energies determined the position of the Compton edge for several sources. These results show that the maximum recoil electron energy is at 89 ± 7 % of the maximum height on the right side of the Compton distribution, when the total charge collected by the detector is used as the energy observable. This result is consistent with simulations carried out with GEANT4 which indicate that, for our geometry of the liquid scintillator detectors, the Compton edge corresponds to the energy at about 90% of maximum in the energy spectrum. Similarly, the maximum in the energy spectrum correspond to 90% of the Compton edge energy [19]. This was assumed to also be the case for BC-537, which could introduce minor systematic uncertainties in the energy calibration if the assumption is not valid. It is worth noting that a recent study of the Compton edge in BC-501A using backscattering in a high-purity germanium detectors places the Compton edge around 80%, which could also induce a systematic uncertainty in the absolute energy scale [40]. To calibrate the detectors, we measured the energy spectra (total charge) of the γ-ray sources as well as the ambient background spectrum without source. The background spectrum was subtracted from the source spectra, normalized to the acquisition time. Simulations predict a complete absorption of the γ rays only for ^{241}Am, due to its low γ-ray energy of 59 keV. The calibration spectra are shown in Fig. 4.

[Figure 4 about here.]

5. Pulse-shape discrimination

Several sophisticated methods for digital pulse-shape discrimination in BC-501A have been developed by various research groups [41–47]. In this work we focus on using ANNs [26, 48]. For BC-537 the literature is more sparse. In Ref. [49] BC-501A and BC-537 were compared using charge comparisons methods and BC-501A was shown to perform better for low energy neutrons. However, no method taking full advantage of digital data analysis, for example a machine-learning algorithms, was implemented in that work.

For this work, the data from the set-up described in section 3 were used. To minimize the influence of different electronics on the results, as well as to evaluate the robustness of the network training, the data sets were collected with the same photomultiplier tube and electronics chain, with only the detector cell itself different. Two methods were applied to evaluate the neutron-γ discrimination capabilities of the two scintillators. The first one was the digital implementation of the charge comparison method and the second ANNs, described in Refs. [25] and [26], respectively. For the charge comparison method, the fast component was chosen to be 15 sampling points, which is the time range 0–30 ns relative to the trigger. The slow component was defined as starting after 30 ns relative to the trigger and have a variable length, extending up to the maximum value of the integral. The integration was stopped when the amplitude of the noise was of the same size as the signal and before electronic artifacts like pulse undershoot had any influence. The pulse shapes from BC-501A and BC-537 are shown in Fig. 2. In the end, the charge comparison pulse-shape discrimination-parameter, C, was calculated as

$$C = \frac{\sum_{t_i=0}^{t_i=30} p(t_i)}{\sum_{t_i=32}^{p(t_i)<0} p(t_i)}, \tag{2}$$

with $p(t_i)$ being the sampled detector pulse amplitude at time t_i.

A feed-forward neural network was created based on the ROOT `TMultiLayerPerceptron` class [50]. It was designed with 75 input nodes, corresponding to the first 75 sampling points after the leading-edge discriminator in the waveform, and two hidden layers of 20 and 5 nodes. An output layer was created with one node where the value 0 corresponds to a γ ray and the value 1 corresponds to a neutron. Each neuron in a layer has its output connected to the input of the neurons in the next layer with a certain weight, w. By adjusting these weights the network can be trained to generate a desired output pattern for a certain input pattern. Furthermore, each neuron has an output activation function, $g(z)$, that normalizes the input, z, into a certain format of the output. In this work we chose the logistic sigmoid function,

$$g(z) = \frac{1}{1 + \mathrm{e}^{-z}}, \tag{3}$$

often used for binary classification problems, such as deciding if a pulse shape corresponds to a neutron or a γ-ray, since it is a smooth function with an output in the range between 0 (γ ray) and 1 (neutron).

Neutrons and γ rays were identified using three-dimensional cuts on total charge (light produced in the scintillator and collected by the photomultiplier tube), TOF, and the analogue pulse-shape discrimination parameter (Z/C signal from the BARTEK NDE202 unit). These cuts were used to select events for training of the ANN. For each scintillator, the network was trained using 50 000 events, and another 50 000 events were used to test it. Of these 100 000 events, about 50 000 were identified as γ rays and 50 000 were identified as neutrons. The test data-set and the training data-set were both part of the training process, randomly chosen in each training epoch. In this way the evolution of the test-data could be followed to avoid over-fitting and the training was stopped when the test data had converged. This training is carried out by minimizing the neural network transfer function with respect to the tensor of individual weights using the Broyden-Fletcher-Goldfarb-Shanno [50–54] method.

The typical error in the training was ~ 8 % for the test data. In Ref. [26], the network was trained using data with 300 MS/s in a time window between 0 and 237 ns (71 sampling points used as input nodes). As we, in this experiment, used 500 MS/s sampling frequency, the time window was limited to between 0 and 150 ns (75 input nodes) in order to keep the size of the network small.

6. Results

6.1. Qualitative results

Qualitative results from the ANN applied to the full data set without pre-selection of neutrons and γ rays are shown in Fig. 5. In this figure the the full data set is shown, as well as events identified as neutrons and γ rays by the ANN. When selecting neutrons with ANNs, the number of γ rays is heavily reduced. This can be observed both in the almost complete disappearance of the vertical band in the distributions with a neutron selection, corresponding to the time independent γ-ray background, as well as the large intensity reduction of the prompt γ-ray peak around TOF = 0. With this selection the neutron distribution is, to a large degree, unaffected. In the γ-selected events almost no neutrons remain for BC-501A, while a small amount of neutrons can be observed in the γ-selected events from BC-537 as a bulge in the flat vertical γ-ray band. This shows that the ANN works well for all events and that the selection of events for training and evaluation does not introduce a bias in the network.

[Figure 5 about here.]

6.2. Quantitative results

To evaluate the results of the discrimination algorithms quantitatively, one-dimensional TOF distributions were used as an observable of the type of incoming radiation. This observable was assumed to be independent of the pulse-shape. In particular, this means that the rising edge of the pulse for a given pulse height is the same both for neutrons and γ rays, and that the exponential decay of the pulse does not influence the CFD properties within experimental sensitivity. Under these assumptions, the performance of the discrimination algorithms should not be biased by the TOF. The number of neutrons within a certain sub-set of the data was estimated by integrating the neutron distribution and subtracting the background at large values of TOF, see Fig. 6. Note that there are two significant assumptions within this estimation. One assumption is that the γ background is time-independent within the 140 ns measurement window, with the exception of the prompt peak. The other assumption is that no neutrons arrive more than 80 ns after the trigger. The first assumption should be uncontroversial while, as seen in Fig. 5, there is a small tail of neutrons at late times that most likely originate from scattering events where the neutrons do not take a straight path. This induces a minor systematic uncertainty in the following quantitative discussion. However, as this uncertainty would affect all data sets equally, a relative comparison between detectors should be unaffected.

[Figure 6 about here.]

The γ-ray suppression efficiency, ϵ_γ, was defined as the fraction of γ rays that was present within a discrimination limit containing $\epsilon_\mathrm{n} = 90\%$ of the neutrons. For a TOF spectrum, $s(t)$, and a discrimination function $f(p)$ (neural network or charge comparison) where $f(p) = 0$ corresponds to a γ ray and $f(p) = 1$ corresponds to a neutron, t being the time bin and p the sampled waveform, an output condition $0 < x < 1$ was defined as,

$$\epsilon_\mathrm{n} = 0.9 = \frac{\sum_{t_i=20}^{80} s(t_i; f(p) > x) - \sum_{t_i=80}^{140} s(t_i; f(p) > x)}{\sum_{t_i=20}^{80} s(t_i) - \sum_{t_i=80}^{140} s(t_i)}, \tag{4}$$

and ϵ_γ was defined as

$$\epsilon_\gamma = \frac{\sum_{t_i=-2}^{4} s(t_i; f(p) > x)}{\sum_{t_i=-2}^{4} s(t_i)}, \tag{5}$$

using x from Eq. (4). Since this definition only includes the fraction of γ rays rejected it is independent of the number of emitted γ rays and neutrons relative to each other. The results are shown in Fig. 7 as a function of light output in electron equivalent keV (keV_{ee}).

[Figure 7 about here.]

One should note, however, that the electron equivalent light output depends on the intrinsic properties of the scintillator, in particular the light output per keV of deposited energy. For γ-rays, this effect is canceled by the calibrations but, for BC-501A, the relation between neutron and γ-rays energy deposition in the scintillator is known to have a non-linear behaviour [55]. Thus, a certain γ-ray energy deposition by a calibration source is not necessarily equivalent to the corresponding neutron energy deposition. The corresponding relation for BC-537 has not been studied. Therefore, data points with the same energy in keV_{ee} do not correspond to the same incoming neutron energy for different scintillators, but should rather be considered as a suppression efficiency for a given γ-ray energy.

While the capability of reducing contamination from a given γ-ray spectrum is one important factor in determining the performance of the different scintillators, another important aspect is how clean the neutron detection will be for a given neutron energy. Due to the non-linearities of the neutron light-output, the translation of measured light into neutron energy is, however, not straightforward. In Ref. [55], the relation between light output originating from electrons, E_{e} and protons, E_{p} has been suggested to be

$$E_{\mathrm{e}} = a_1 E_{\mathrm{p}} - a_2 \left(1 - \exp\left(-a_3 E_{\mathrm{p}}^{a_4}\right)\right), \tag{6}$$

for the scintillators NE-102, NE-213, NE-224, NE-228, and NE-228A. Similar values of the parameters, a_i, from Ref. [55] were obtained in Ref. [56] where the light response of BC-501A was measured as a function of both E_{p} and deuteron energy, E_{d}. We have used the parameters for deuteron-proton scattering in BC-501A to approximate the neutron-deuteron scattering, E_{d}, in BC-537. While the validity of Eq. (6) should be strongly correlated between NE-213 and BC-501A, as these are equivalent liquids from different producers, it has not been validated for BC-537 or any of its equivalents. However, as the light output is a consequence of atomic interactions of the proton/deuteron within the liquid and the atomic structure should be isotope independent, we assume a validity of Eq. (6) also for BC-537 based on its validity in the deuteron interaction in BC-501A from Ref. [56].

The parameters used are listed in Table 2, and the results are shown in Fig. 8. These parametrizations give results consistent with the GEANT4 simulations in Ref. [19], in particular Fig. 14 of Ref. [19], where the light output of the two scintillators were evaluated using a simulated pencil beam of 2 MeV neutrons. Experimentally, the response functions for neutrons in EJ-301 has been measured using TOF from a deuterium-tritium neutron generator and evaluated using both the exponential parametrization in Eq. (6) and a polynomial parametrization [57]. The results from that evaluation shows a reasonable agreement with the coefficients used in this work, within error bars.

[Table 2 about here.]

[Figure 8 about here.]

7. Summary and conclusions

The results show that, using the charge comparison method, BC-501A has a higher γ-ray rejection efficiency, ϵ_γ, than BC-537 over the energy range 100-1000 $\mathrm{keV_{ee}}$. This can be explained by that, for the same energy, BC-501A gives larger light output than BC-537. The discrimination between neutrons and γ rays using ANNs, however, gives more than 95% γ-ray suppression efficiency down to a γ-energy of around 150 $\mathrm{keV_{ee}}$ for both BC-501A and BC-537. Thus, using ANNs, most of the γ-ray spectrum can be almost completely suppressed in a neutron detector array.

When translating this energy into an estimated energy scale of proton/deuteron interactions, the lower light output of BC-537 causes a higher cut-off energy for separating neutrons and γ rays. While the ANN in this particular test has a larger ϵ_γ than the charge comparison in both BC-501A and BC-537, the energy cut-off for neutrons in the BC-501A case is at around 800 $\mathrm{keV_{pe}}$ while the cut-off in BC-537 was at around 1200 $\mathrm{keV_{de}}$. This is a significant disadvantage for BC-537 as, due to scattering kinematics, a large fraction of the events will occur at low energies.

These results were obtained by collecting data using two identical detectors of each type. The neural network was trained using data from one of the detectors and evaluated using data from the other detector. This shows that the ANNs are indeed robust enough to apply a single network to different detectors, a property that will be important for implementation in high-granularity arrays.

Acknowledgements

This work was partially financed by the Swedish Research Council, UK Science and Technology Facilities Council (STFC) under grant numbers ST/J000124/1, ST/L005727/1, and ST/L005735/1, NuSTAR.DA BMBF 05P15RDFN1, 114F473 for TUBITAK, and the Polish National Research Centre under contracts no. 2013/08/M/ST2/00257 (LEA-COPIGAL) and 2016/22/M/ST2/00269. A.Gadea activity has been partially supported by MINECO and Generalitat Valenciana, Spain, grants FPA2014-57196-C5, Severo Ochoa and PROMETEO II/2014/019 and by the E.C. FEDER funds. G. Jaworski acknowledges the support of the framework of the European Social Fund through the Warsaw University of Technology Development Programme, realised by the Center for Advance Studies. We would also like to thank Mr. A. Grant and Mr. I. Burrows from the STFC Daresbury Laboratory for the CAD drawings used for Fig. 1.

References

[1] E. Clément et al., Nucl. Instr. Meth. A855 (2017) 1.

[2] F. Camera et al., Rom. Rep. Phys. 68 (2016) S539.

[3] N. Warr et al., Eur. Phys. J. A49 (2013) 40.

[4] G. Bisoffi et al., Nucl. Instr. Meth. B376 (2016) 402.

[5] N. Lalović et al., Nucl. Instr. Meth. A806 (2016) 258.

[6] M. Lebois et al., Nucl. Instr. Meth. A735 (2014) 46.

[7] S. M. Lenzi et al., Phys. Rev. Lett. 87 (2001) 122501.

[8] A. Gadea et al., Phys. Rev. Lett. 97 (2006) 152501.

[9] B. Cederwall et al., Nature 469 (2011) 68.

[10] M. Palacz et al., Phys. Rev. C 86 (2012) 014318.

[11] F. Ghazi Moradi et al., Phys. Rev. C 89 (2014) 014301.

[12] F. Ghazi Moradi et al., Phys. Rev. C 89 (2014) 044310.

[13] T. Hüyük et al., Eur. Phys. J. A52 (2026) 55.

[14] J.N. Scheurer et al., Nucl. Inst. Meth. A385 (1997) 510.

[15] S. Akkoyun et al., Nucl. Instr. Meth. A668 (2012) 26.

[16] D. Testov et al., in: S. Canella and R. Pengo (Ed.), LNL Annual Report 2014, 2015, p. 73.

[17] P. E. Garrett et al., Hyperfine Int. 225 (2014) 137.

[18] J. J. Valiente Dobón et al., submitted to Nucl. Inst. Meth. A.

[19] G. Jaworski et al., Nucl. Inst. Meth. A673 (2012) 64.

[20] X. L. Luo et al., Nucl. Inst. Meth. A767 (2014) 83.

[21] V. Modamio et al., Nucl. Inst. Meth. A775 (2015) 71.

[22] F. J. Egea et al., IEEE Trans. Nucl. Sci. 60 (2013) 3526.

[23] F. J. Egea Canet et al., IEEE Trans. Nucl. Sci. 62 (2015) 1063.

[24] F. J. Egea Canet et al., IEEE Trans. Nucl. Sci. 62 (2015) 1056.

[25] P.-A. Söderström, J. Nyberg, R. Wolters, Nucl. Inst. Meth. A594 (2008) 79.

[26] E. Ronchi et al., Nucl. Inst. Meth. A610 (2009) 534.

[27] J. Ljungvall et al., Nucl. Inst. Meth. A528 (2004) 741.

[28] J. Cederkäll et al., Nucl. Inst. Meth. A385 (1996) 166.

[29] V. Bildstein et al., Nucl. Instr. Meth. A792 (2013) 188.

[30] J. Qin et al., Appl. Radiat. Isot. 1041 (2015) 15.

[31] F. T. Kuchnir, F. J. Lynch, IEEE Trans. Nucl. Sci. NS-15 (1968) 107.

[32] W. F. Caplehorn, G. P. Rundle, Proc. Phys. Soc. A 64 (1951) 546.

[33] M. Moszynski et al., Nucl. Instr. Meth. A350 (1994) 226.

[34] M. Moszynski et al., Nucl. Instr. Meth. A307 (1991) 97.

[35] Ö Skeppstedt et al., Nucl. Inst. Meth. A421 (1999) 531.

[36] `http://www.struck.de/sis3350.htm`, accessed 2018-10-01.

[37] `http://www.struck.de/sis3302.htm`, accessed 2018-10-01.

[38] J. Agramunt, A triggerless digital data acquisition system for nuclear decay experiments, Master's thesis, Unvesitat de Valencia, Valencia (2012).

[39] H. H. Knox, T. G. Miller, Nucl. Inst. Meth. 101 (1972) 519.

[40] L. Swiderski et al., Radiat. Meas. 45 (2010) 605.

[41] S. Marrone et al., Nucl. Instr. and Meth. A490 (2002) 299.

[42] C. Guerrero et al., Nucl. Inst. Meth. A597 (2008) 212.

[43] N. V. Kornilov et al., Nucl. Inst. Meth. A497 (2003) 467.

[44] D. Savran et al., Nucl. Inst. Meth. A624 (2010) 675.

[45] X. Luo, G. Liu, Yang, in: Proceedings of the 2010 1st International Conference on Pervasive Computing, Signal Processing and Applications, PCSPA 2010, IEEE, 2010, p. 994.

[46] B. D'Mellow et al., Nucl. Inst. Meth. A578 (2007) 191.

[47] M. D. Aspinall et al., Nucl. Inst. Meth. A583 (2007) 432.

[48] G. Liu et al., Nucl. Inst. Meth. A607 (2009) 620.

[49] C. Xiaohui et al., Nucl. Inst. Meth. A694 (2012) 111.

[50] `http://root.cern.ch/root/html/TMultiLayerPerceptron.html`, accessed 2018-10-01.

[51] C. G. Broyden, J. Inst. Maths. Appl. 6 (1970) 76.

[52] R. Fletcher, Comput. J. 13 (1970) 317.

[53] D. Goldfarb, Math. Comp. 24 (1970) 23.

[54] D. F. Shanno, Math. Comp. 24 (1970) 647.

[55] R. A. Cecil, B. D. Anderson, R. Madey, Nucl. Inst. Meth. 161 (1979) 439.

[56] N. Nakao et al., Nucl. Instr. Meth. A362 (1995) 454.

[57] L. Iwanowska et al., Nucl. Inst. Meth. A781 (2015) 44.

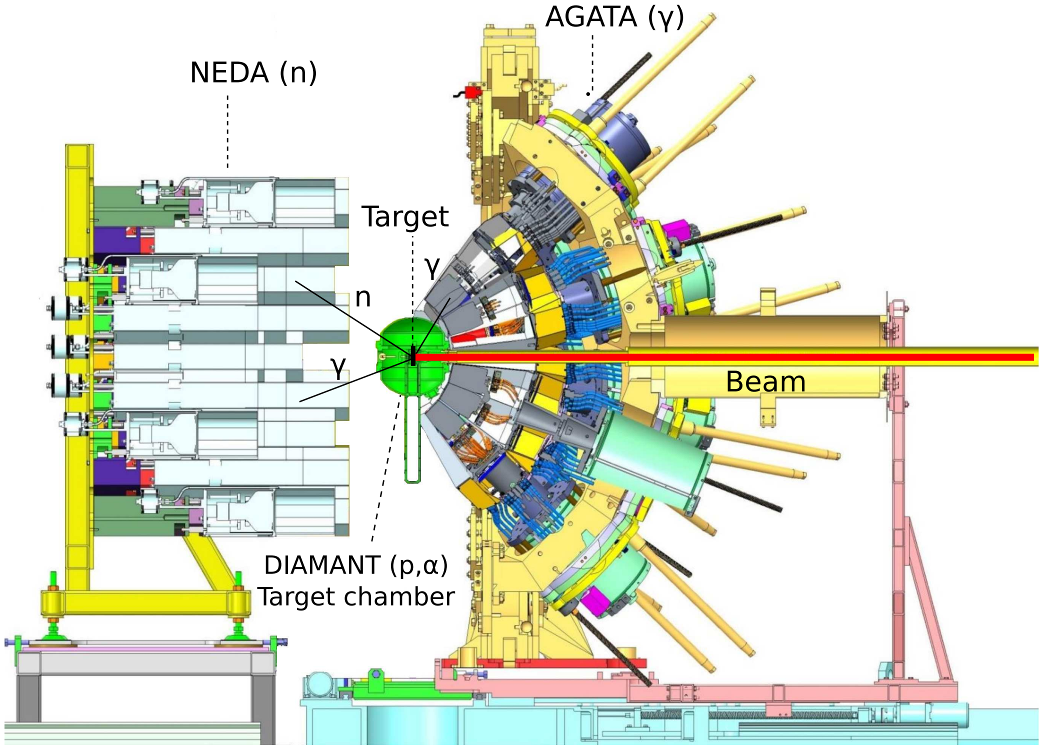

Figure 1: Illustration of a typical set-up for heavy-ion fusion-evaporation experiments, adapted from the NEDA [13], DIAMANT [14] and AGATA [15] campaign at GANIL [1]. Following the fusion of a nucleus from a heavy-ion beam with a nucleus from the experimental target, the compound nucleus is identified based on the sum of the beam and target isotopes, minus the evaporation residues like charged particles detected in CsI scintillator detectors (DIAMANT) and neutrons detected in neutron detectors (NEDA). The structure of the compound nucleus is then studied by the characteristic γ radiation detected in the HPGe γ-ray spectrometer (AGATA). Also illustrated is the possible misidentification of the reaction channel due to interactions of γ rays in the neutron detector system.

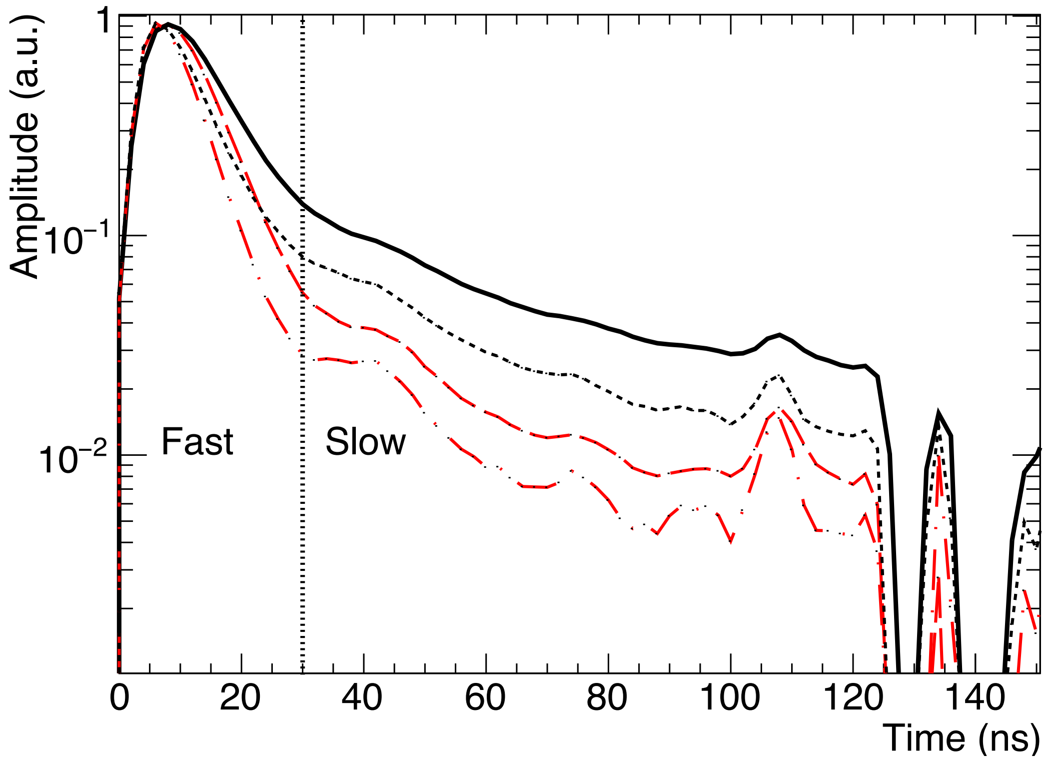

Figure 2: (Colour online.) Average pulse shapes from BC-501A (black, solid and dotted) and BC-537 (red, long dashed and dash-dotted) for neutrons (solid and long dashed) and γ rays (dotted and dash-dotted). Neutrons and γ-rays were selected according to the 3D cuts described in section 5. A small reflection in the electronics can be seen at 110 ns.

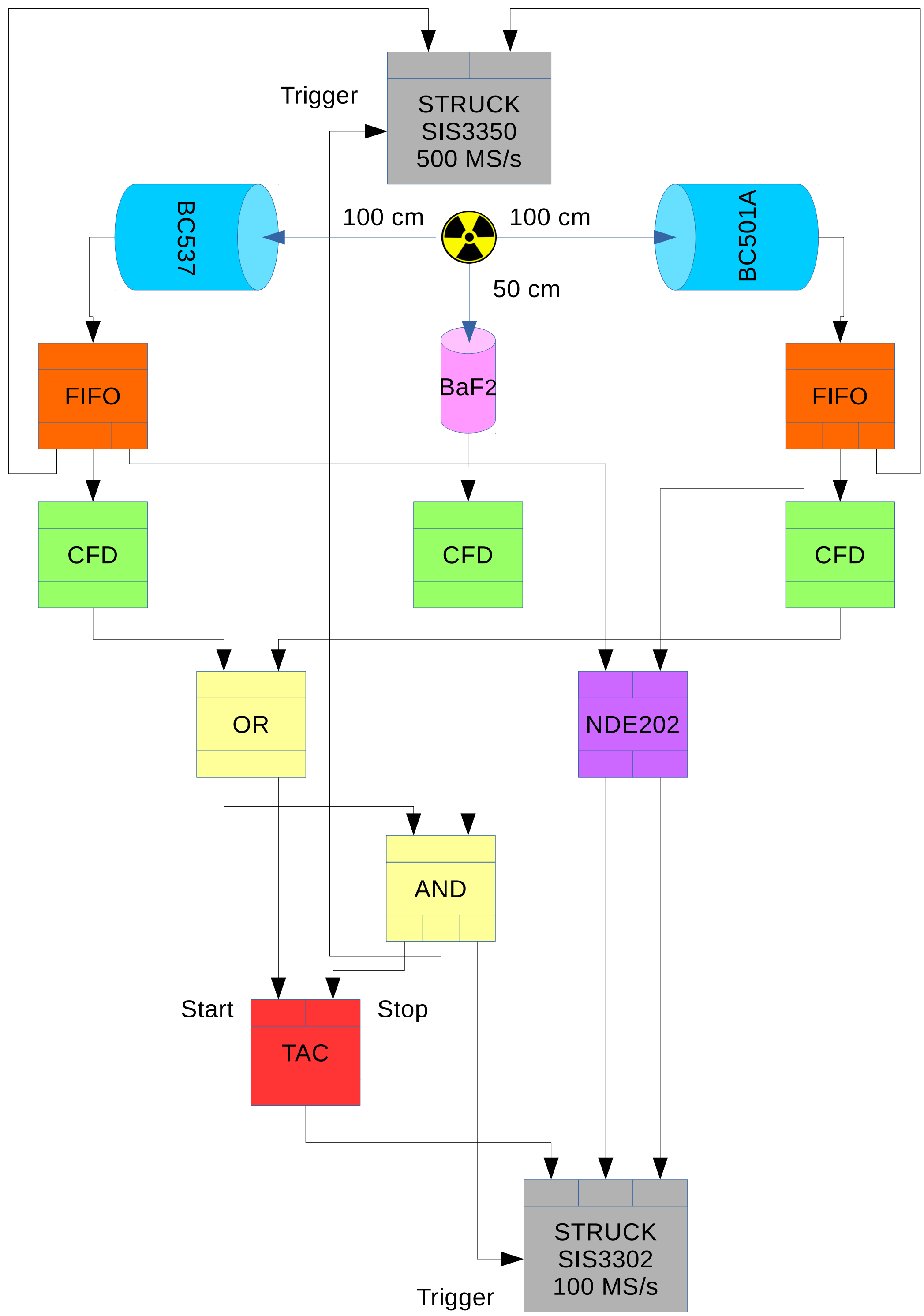

Figure 3: Illustration of the experimental set-up.

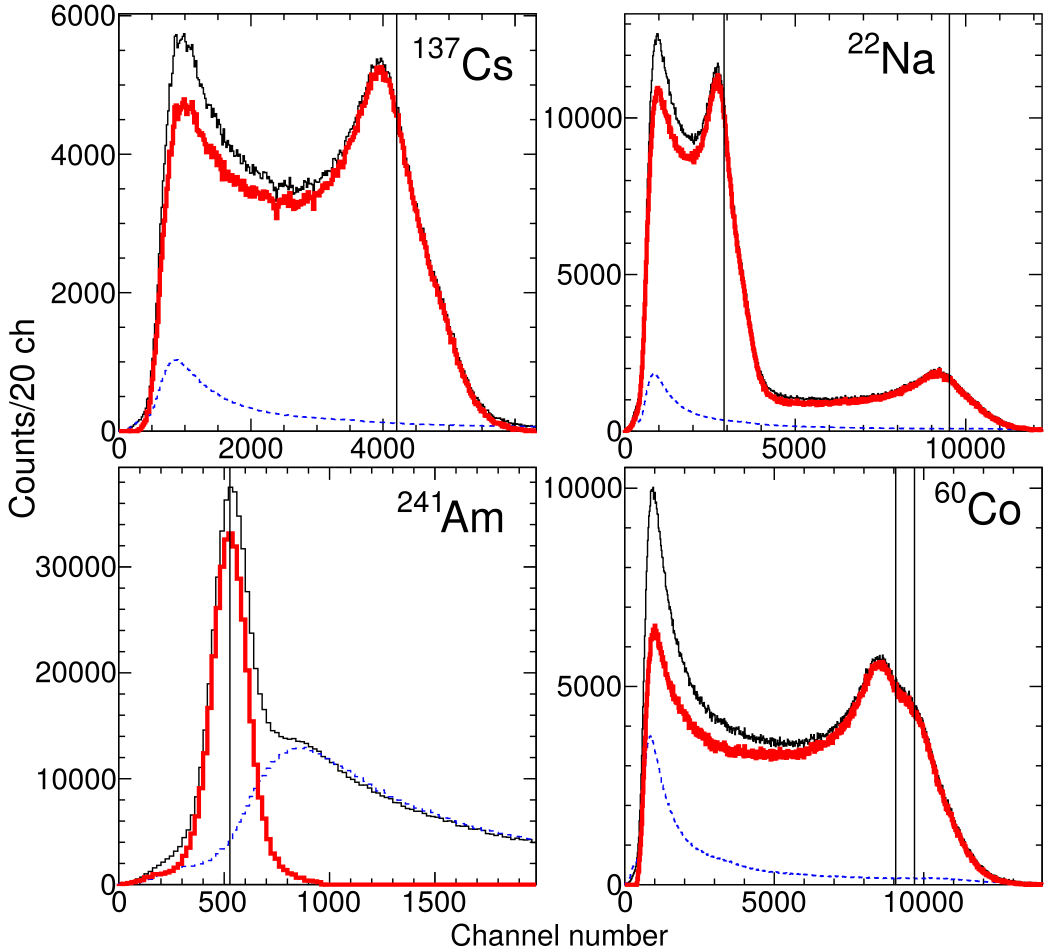

Figure 4: (Colour online.) Energy spectra (black, thin) obtained with four different calibration sources. The ambient γ-ray room background collected without source (blue, dotted) is shown in each panel together with the background subtracted energy signal (red, thick). For each source also the location of the Compton edges, assumed to be at 90% of the maximum, is shown. For ^{241}Am, the location of the full-energy deposition peak is shown instead of the location of the Compton edge.

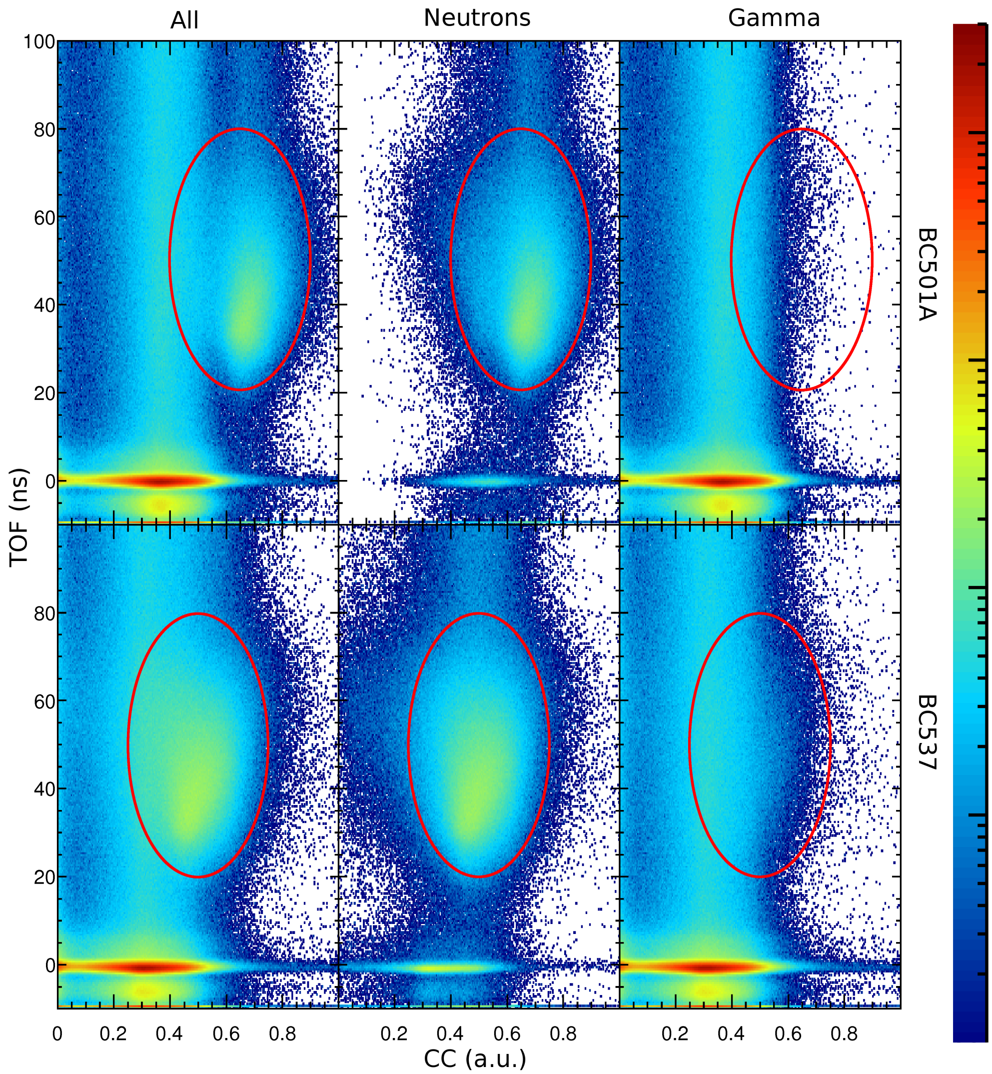

Figure 5: (Colour online.) Two-dimensional plots in logarithmic scale of time-of-flight versus digital charge comparison (CC) for the full data set (left), selected on neutrons (middle) and γ rays (right) for BC-501A (top) and BC-537 (bottom) using the artificial neural network. The locations of the neutron distributions are shown as red circles.

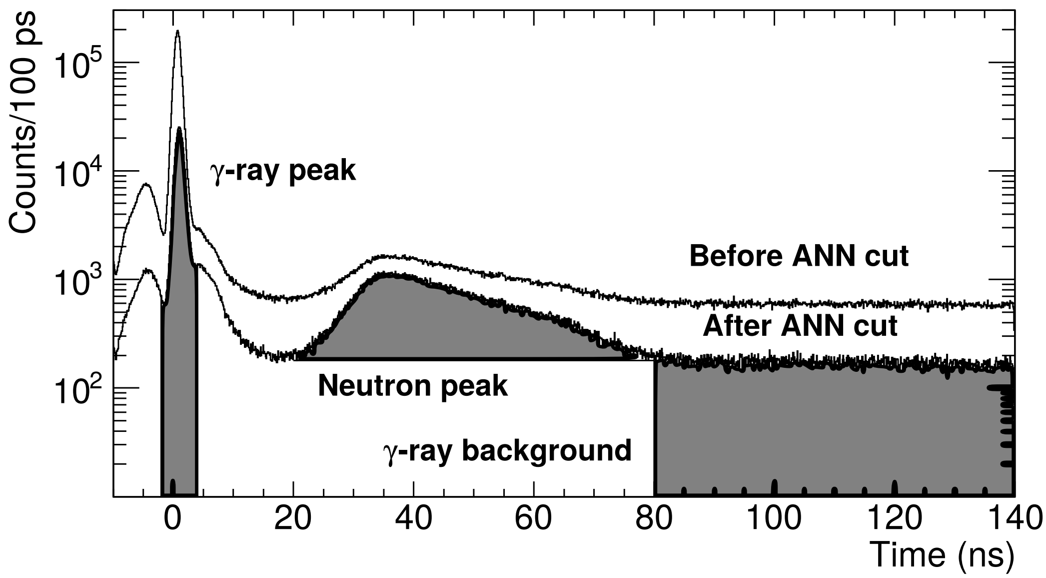

Figure 6: Time-of-flight spectrum used for quantification of the γ-suppression efficiency of the full data set, and after applying an artificial neural network with a 90% neutron requirement. Shaded areas show the γ-ray peak, the neutron distribution and the region used for background subtraction, respectively.

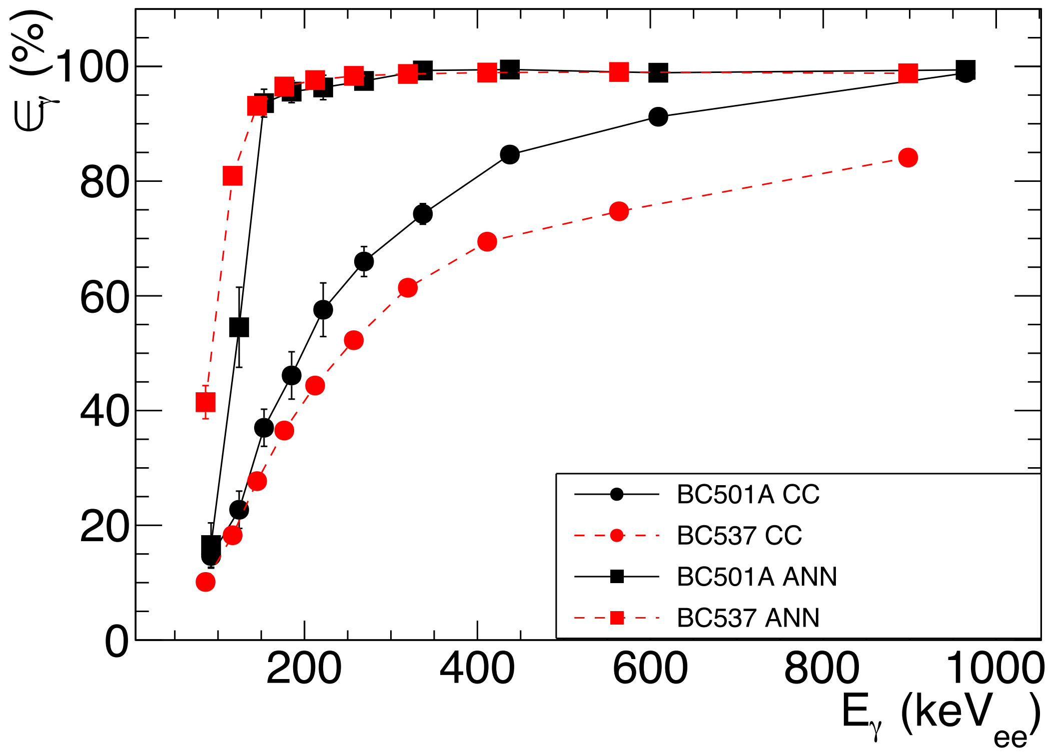

Figure 7: (Colour online.) Rejection efficiency of γ rays for a pulse-shape discrimination gate that contains 90 % of the neutrons. BC-501A is shown in black and BC-537 in red. The two discrimination algorithms are: artificial neural networks (squares) and charge comparison (circles).

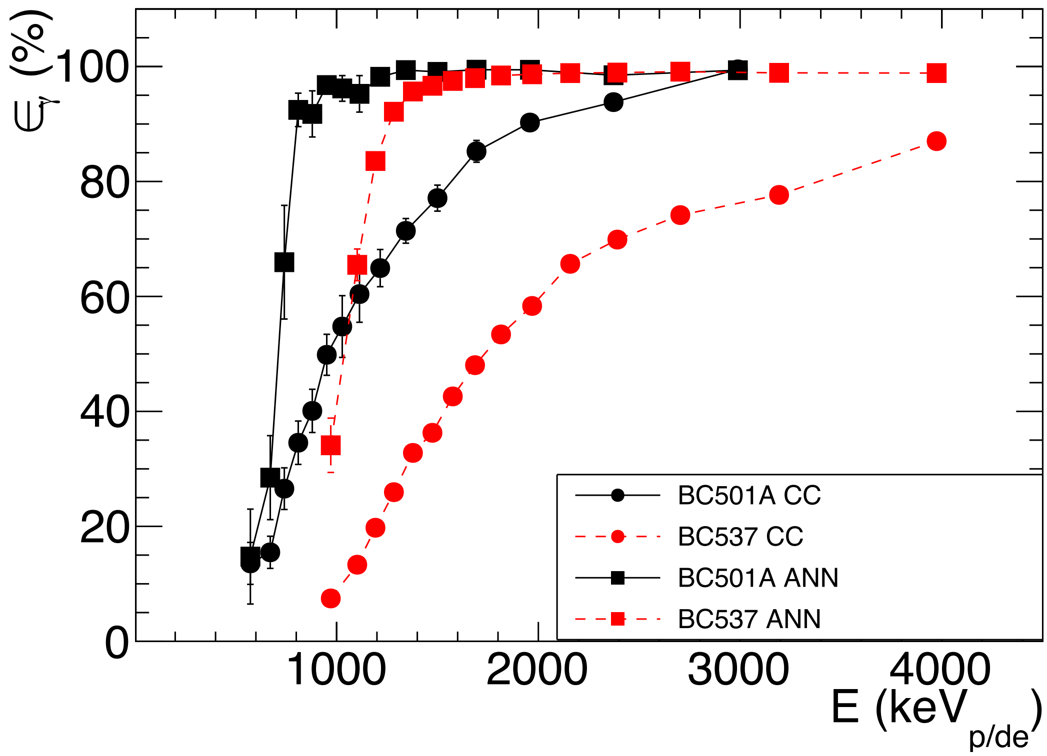

Figure 8: (Colour online.) Same as Fig. 7, with the energy scale adjusted to equivalent proton/deuteron energy keV$_{\mathrm{p/de}}$.

Table 1: Properties of the γ-ray sources used for calibration of the liquid scintillators. Due to the poor energy resolution of the scintillators, the average energy was used for the two ^{60}Co lines, denoted by *.

Source	γ-ray energy (keV)	Compton edge (keV)	Main energy loss mechanism
^{22}Na	511	341	Compton
^{22}Na	1275	1062	Compton
^{137}Cs	622	441	Compton
^{60}Co	1173*	963*	Compton
^{60}Co	1332*	1118*	Compton
^{241}Am	59	-	Photoelectric

Table 2: Parameters used for converting keV_{ee} into $\text{keV}_{\text{p/de}}$. Note that the parameter a_4 marked with * is not included in Ref. [56], but assumed to be the same as in Ref. [55]. The corresponding light output for a 2 MeV neutron pencil-beam is included for comparison with the GEANT4 simulations in Ref. [19].

Liquid	a_1	a_2	a_3	a_4	$E_{\text{n}} = 2$ MeV (keV_{ee})
BC-501A	0.83	2.82	0.25	0.93	591
BC-537	0.75	4.5	0.16	0.93^*	318